The Origin of Fluorescence from Graphene Oxide

Jingzhi Shang[1], Lin Ma[1], Jiewei Li[1,2], Wei Ai[1,2], Ting Yu[1,3,4,†] and Gagik G. Gurzadyan[1,†]

[1]Division of Physics and Applied Physics, School of Physical and Mathematical Sciences, Nanyang Technological University, Singapore 637371

[2]Key Laboratory for Organic Electronics & Information Displays (KLOEID) and Institute of Advanced Materials (IAM), Nanjing University of Posts and Telecommunications, Nanjing 210046, China

[3]Department of Physics, Faculty of Science, National University of Singapore, Singapore 117542

[4]Graphene Research Centre, National University of Singapore, 2 Science Drive 3, Singapore 117542
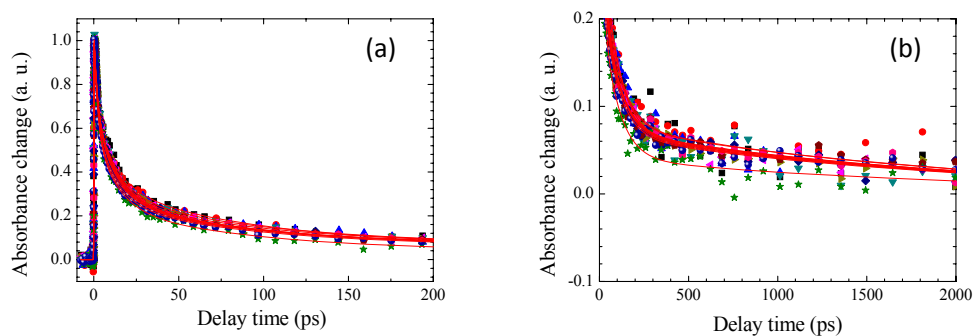
Figure S1 Normalized kinetic curves of graphene oxide (GO) in water at probe wavelengths between 560 and 760 nm measured by transient absorption spectroscopy. (a) and (b) show the decay curves in the first 200 ps and the decay tails up to 2000 ps, respectively. Experimental data and fit curves denoted by scatters and red lines, respectively.
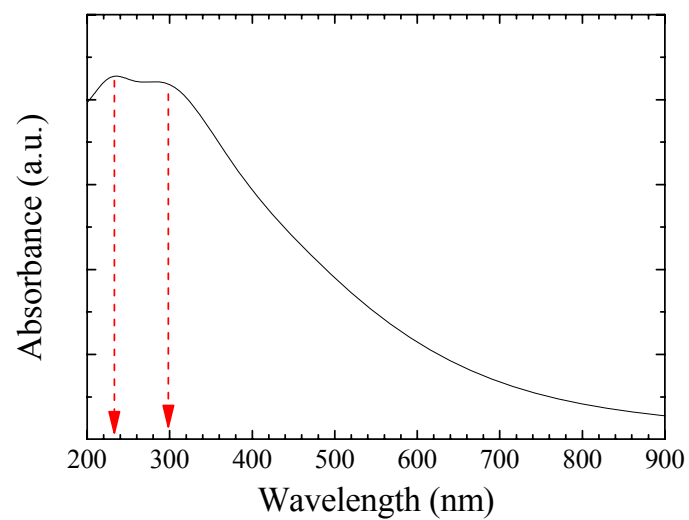
Figure S2 Simulated absorption spectrum of GO in the range from 200 to 900 nm

(Material studio 5.5 Dmol3 module)
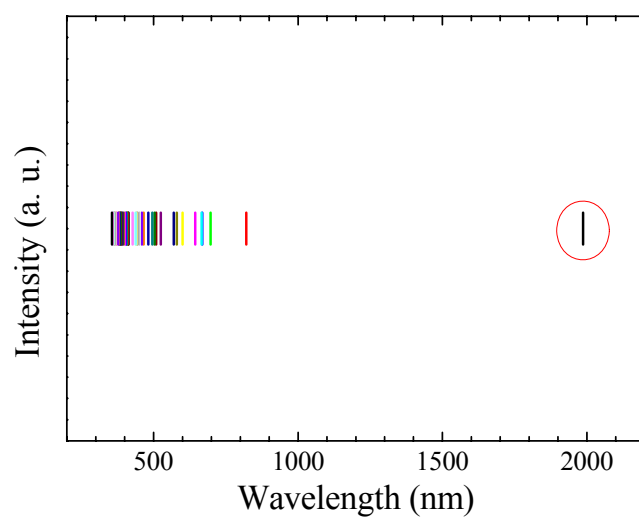
Figure S3 Calculated absorption wavelengths of GO; the band edge absorption wavelength is indicated by red circle

(Material studio 5.5 Castep module)
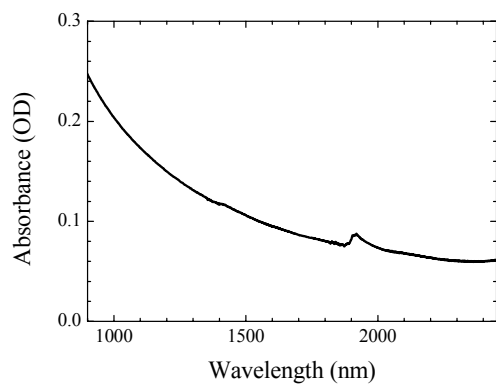
Figure S4 Near infrared absorption spectrum of GO film on quartz substrate
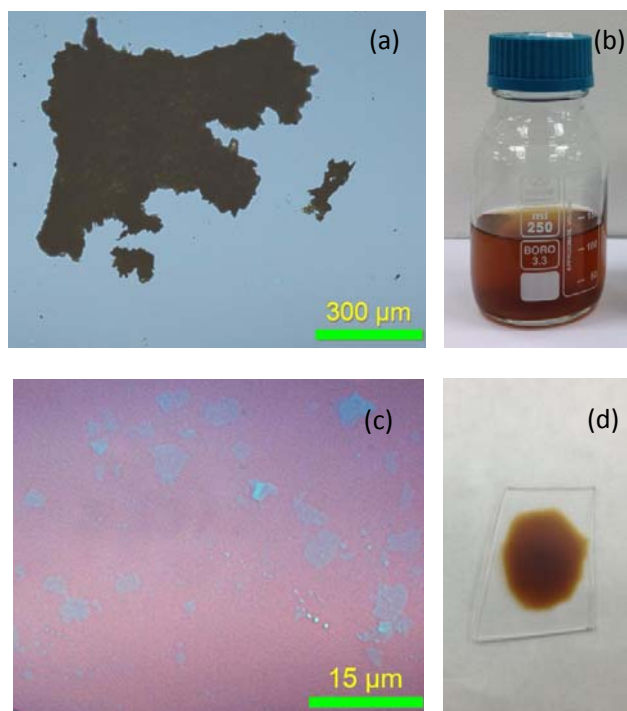
Figure S5 Optical images of (a) graphite oxide, (b) GO in water, (c) GO on SiO$_2$/Si wafer and (d) GO film on quartz, respectively.

3
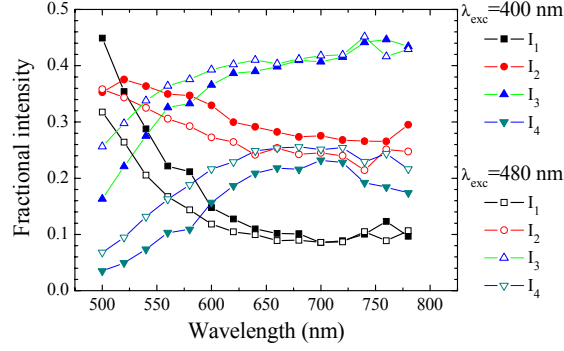
Figure S6 Fractional intensities of four lifetime components

The fractional intensities (I_i, i=1,2,3,4) of four lifetime components (as shown in Figure S6) were calculated by use of the fractional amplitudes and lifeimes (A_i and τ_i, i=1,2,3,4) in Figure 4d:

$$I_i = \int_0^\infty A_i e^{-\frac{t}{\tau_i}} dt = A_i \tau_i \qquad \text{(Eq. S1)}$$

and

$$I_1 = \tau_1 {}^* A_1 / (\tau_1 {}^* A_1 + \tau_2 {}^* A_2 + \tau_3 {}^* A_3 + \tau_4 {}^* A_4);$$

$$I_2 = \tau_2 {}^* A_2 / (\tau_1 {}^* A_1 + \tau_2 {}^* A_2 + \tau_3 {}^* A_3 + \tau_4 {}^* A_4);$$

$$I_3 = \tau_3 {}^* A_3 / (\tau_1 {}^* A_1 + \tau_2 {}^* A_2 + \tau_3 {}^* A_3 + \tau_4 {}^* A_4);$$

$$I_4 = \tau_4 {}^* A_4 / (\tau_1 {}^* A_1 + \tau_2 {}^* A_2 + \tau_3 {}^* A_3 + \tau_4 {}^* A_4). \qquad \text{(Eq. S2)}$$

And then, the fluorescence intensities of four lifetime components (Figure 5) were extracted by multiplying the total fluorescence by I_i, respectively.

Therefore, according to Eqs (S1, S2), the contributions to the steady-state fluorescence vary proportionaly to the lifetimes and fractional amplitudes, which means the contribution of τ_1 (the shortest lifetime) should be the smallest. However, since the fractional amplitude of τ_1 is large in 500-600 nm region, therefore the contribution to steady-state fluorescence of τ_1 is also quite high (Figure 5).
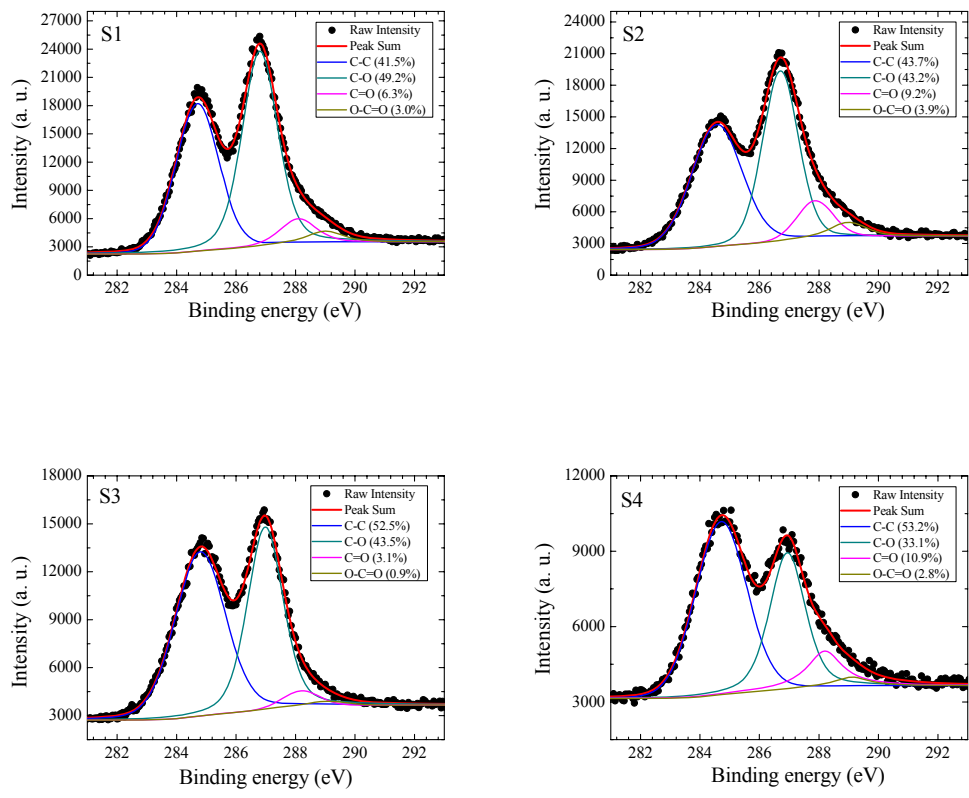
Figure S7. XPS spectra of GO samples: S1-S4.
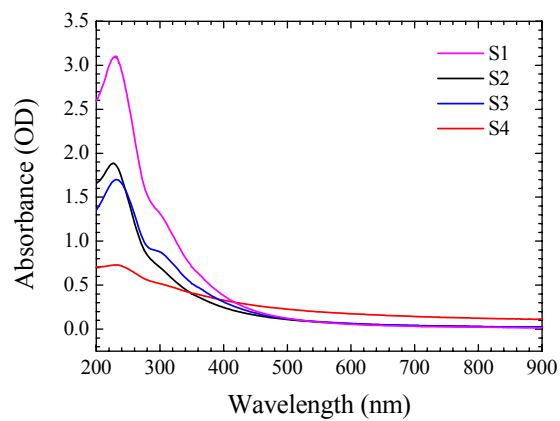
Figure S8. Absorption spectra of GO samples, S1-S4, in 2 mm quartz cuvettes. From S1 to S4, the absorbance decreases in short wavelengths. S4 shows a higher absorbance in the visible and NIR regions.
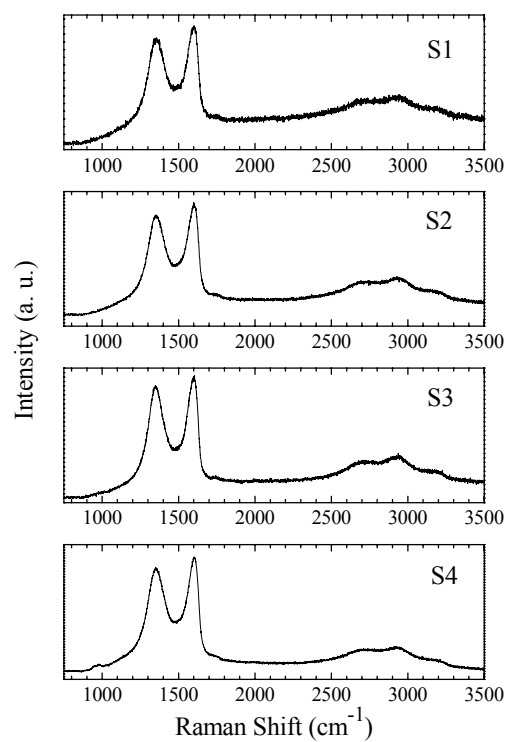
Figure S9. Raman spectra of GO samples: S1-S4. Four samples show the similar features.
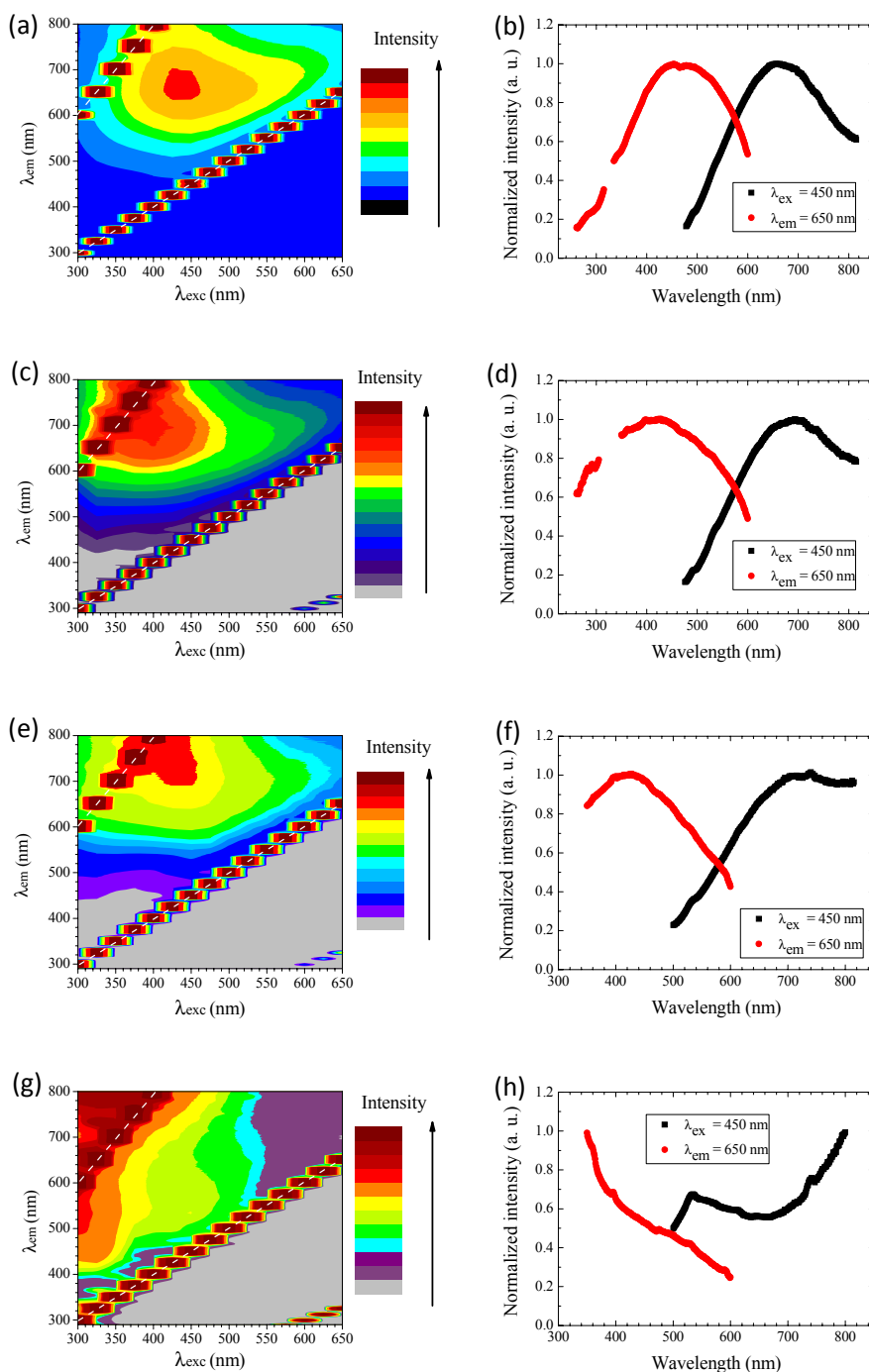
Figure S10 (a, c, e, g) fluorescence excitation-emission maps of GO samples S1-S4, respectively; the corresponding fluorescence maxima are located at ~670, ~700, ~730 and ~530 nm, respectively. (b, d, f, h) Fluorescence excitation and emission spectra of GO samples S1-S4, respectively. Different fluorescence emission and excitation maxima were observed. From S1 to S3, the emission/excitation maximum redshifts/blueshifts.
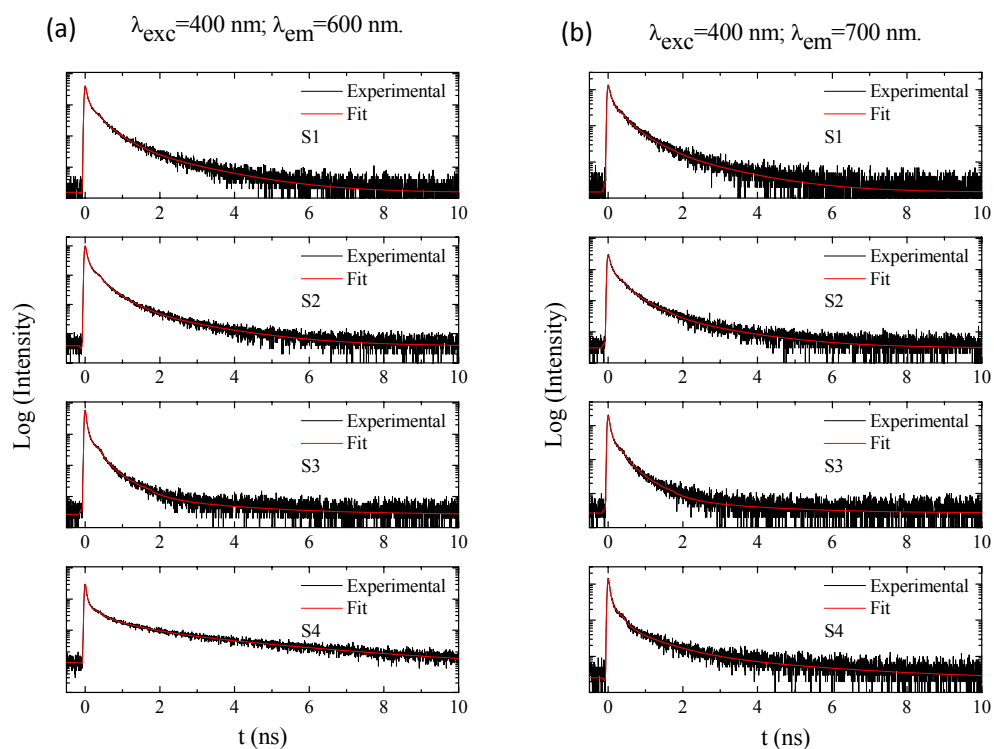
Figure S11 Fluorescence decay curves of samples S1-S4 at (a) 600 and (b) 700 nm, respectively.
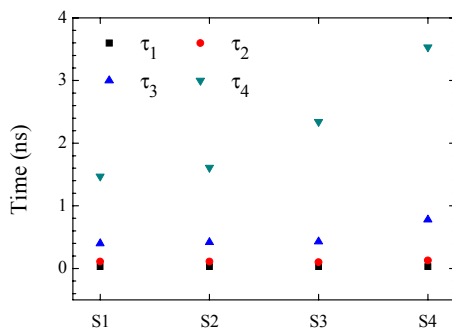
Figure S12 Decay times of samples S1-S4 obtained by global fit of TCSPC measurements, respectively. For S1-S3, the first three decay times (τ_1, τ_2 and τ_3) are quite similar and the last component (τ_4) slowly increases. For S4, the first two time components (τ_1 and τ_2) are similar to those of S3 while the last two (τ_3 and τ_4) are higher than those of S3.
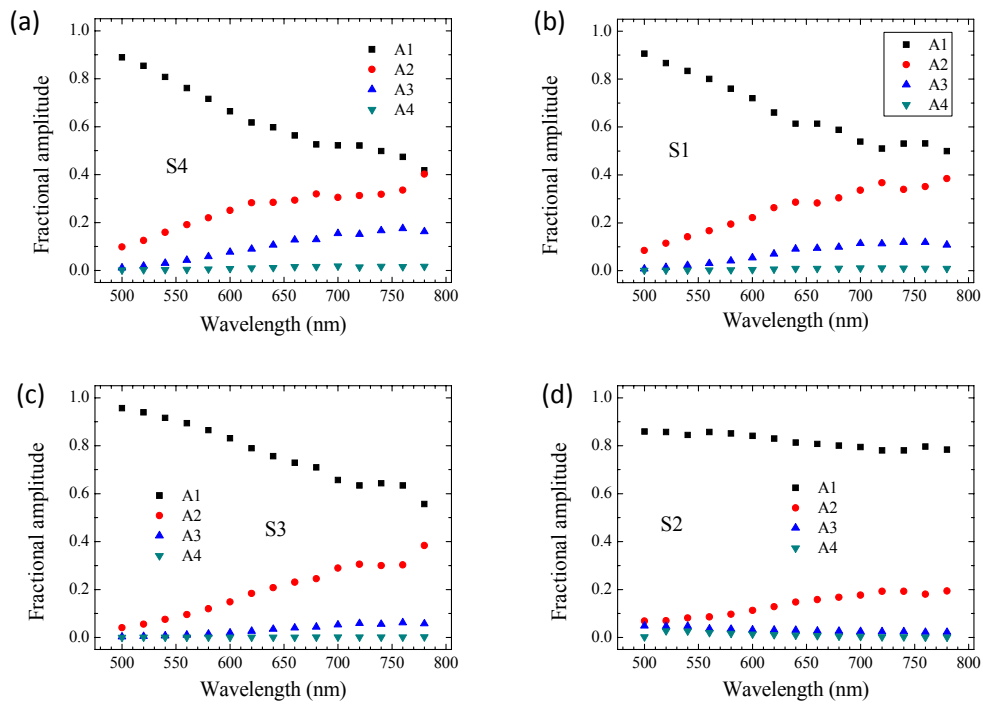
Figure S13 Fractional amplitudes of decay times of samples S1-S4 at 600 (left) and 700 nm (right), respectively. Changes of amplitudes of four time components were observed for S1-S4.
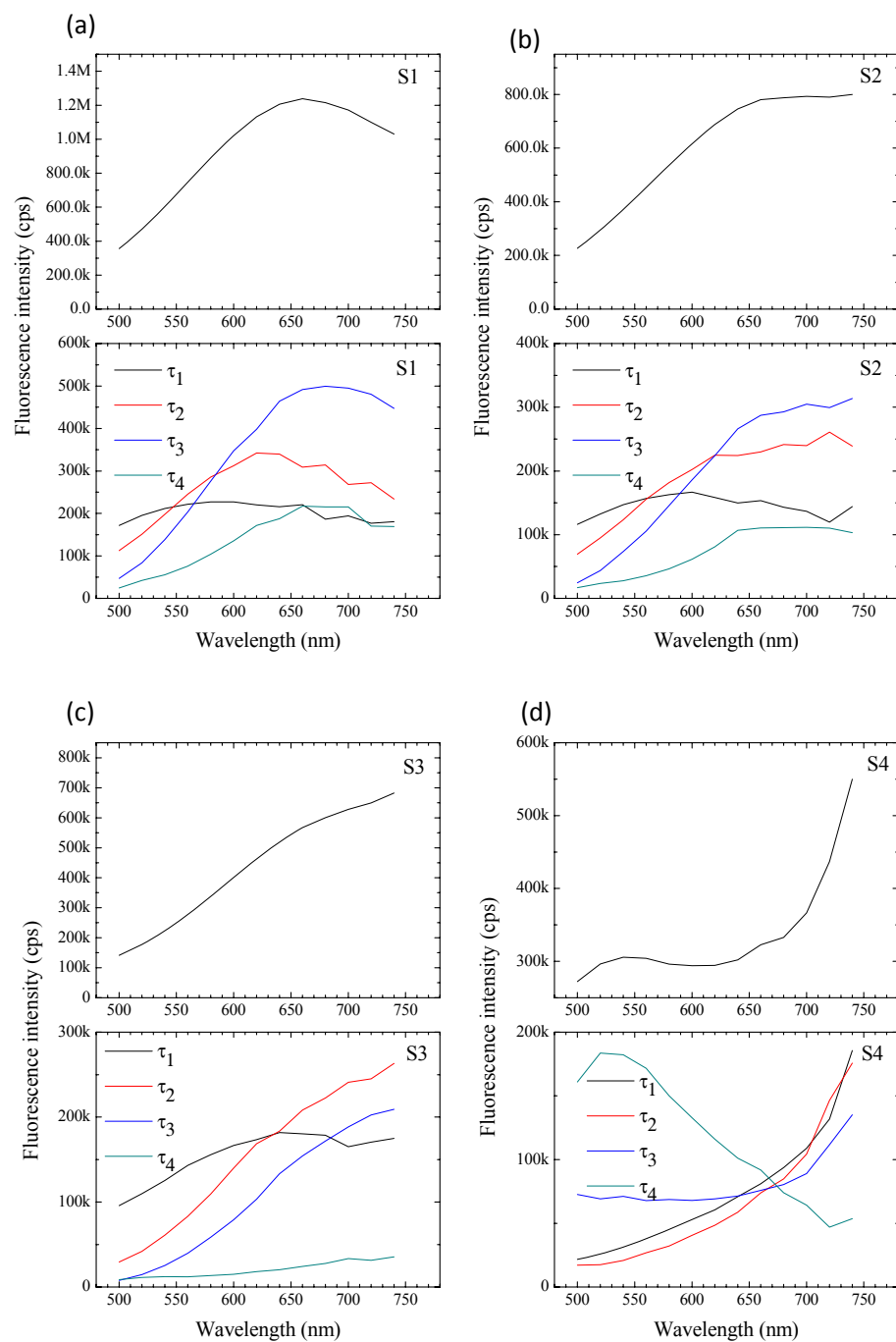
Figure S14 Fractional fluorescence peaks of samples S1-S4 at 400 nm excitation, respectively. For S1-S3, the relative contributions of four components vary with the proportions of bonds in GO. For S4, the time component ($\tau 4$) contributes most to the emission band between 500 and 600 nm.
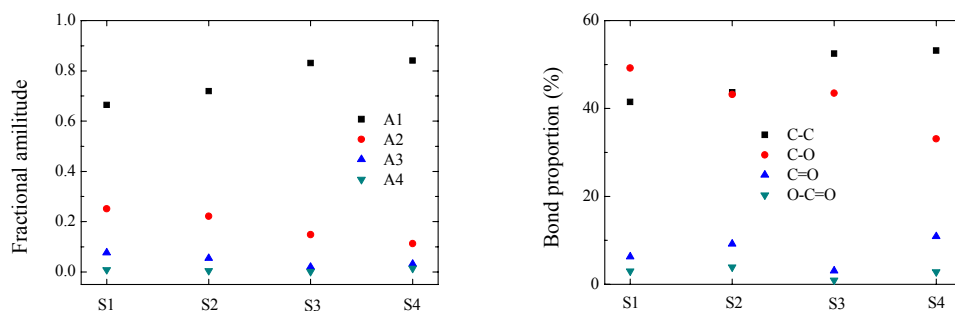
Figure S15 (a) Fraction amplitudes of time components (τ_1- τ_4) of S1-S4 at 600 nm; (b) Proportions of C-C, C-O, C=O and O-C=O in S1-S4.

From TCSPC measurements, we found a strong correlation between excited state lifetimes for S1-S4 and proportions of functional groups (Figures S12 and S13). This obviously excludes participation of the states induced by random disorder. This could be a hint that the fluorescence is from the partial regions in these samples rather than from the whole structure. It is consistent with the proposed multiple chromophore/fluorophore system, localized at non-oxidized areas and boundaries between oxidized and non-oxidized regions.
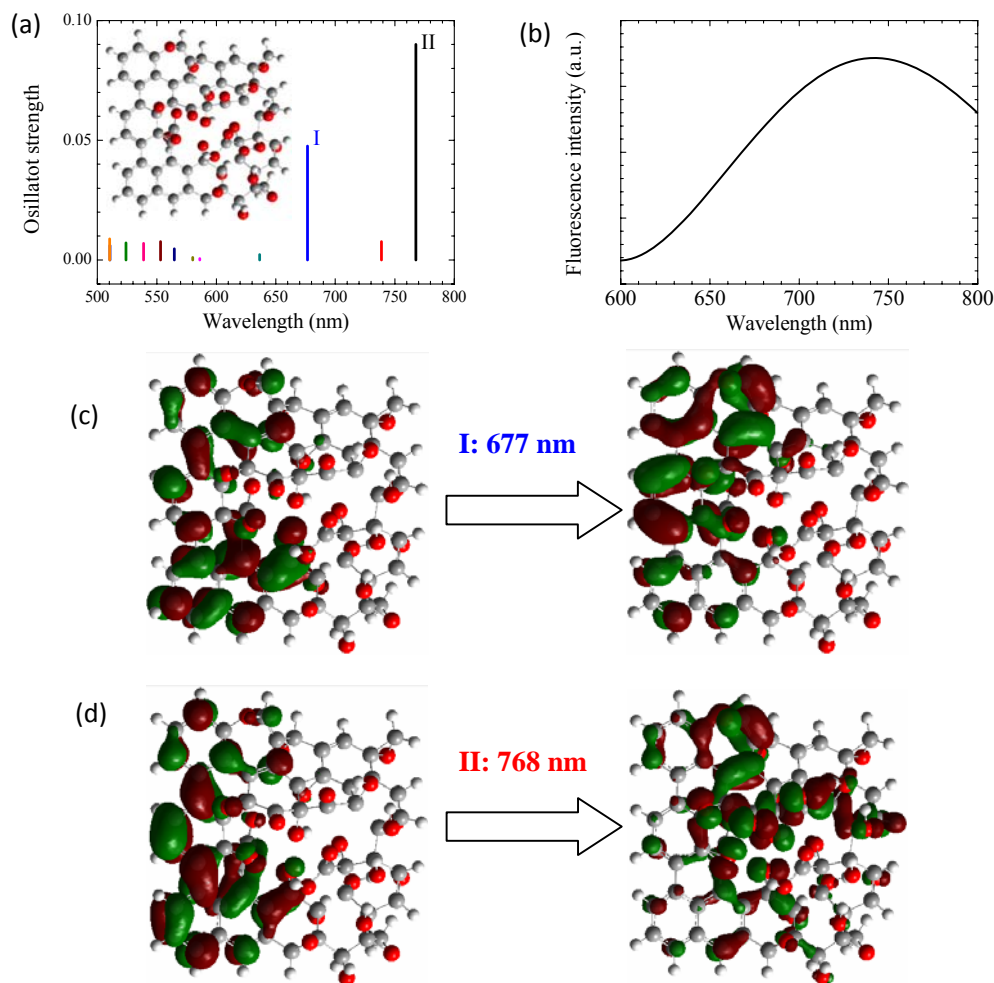
Figure S16 (a) Calculated oscillator strengths for optical emission of a simplified structural model, a single GO cell with edges terminated by H atoms as shown in the inset (C: gray; O: red; H white); there are two strong transitions (I, II) at 677 and 768 nm, respectively; (b) Simulated fluorescence spectrum of this single molecular structure; (c, d) Optical emission related orbitals at 677 nm and 768 nm of this simplified structural model, respectively. These calculations are based on Gaussian 09 software at the B97D/TZVP level[SR1,SR2]. Similar simulations of a graphene fragment with COOH and COO$^-$ were also performed in Ref. 19.

(Gaussian(R) 09 program)

Supplementary References:

SR1. Grimme, S. Accurate description of van der Waals complexes by density functional theory including empirical corrections. *J. Comput. Chem.* **25** (12), 1463 (2004).

SR2. Peverati, R. & Baldridge, K. K. Implementation and performance of DFT-D with respect to basis set and functional for study of dispersion interactions in nanoscale aromatic hydrocarbons. J. *Chem. Theory Comput.* **4** (12), 2030-2048 (2008).